Research on reflection properties of Ag-AAO-Al microstructures

YONG CAI, SHULING HOU, HUIYING ZHOU[*]
School of Computer and Information Engineering, Central South University of Forestry Science and Technology, Changsha 410004, China

The reflection spectra of the microstructures with different AAO thickness, different AAO pore size and different kinds of liquids in AAO films were obtained experimentally and simulated based on COMSOL at the perpendicular incidence of 450-1150 nm. The results show that the variation of reflection spectra of the Ag-AAO-Al microstructure depends on the thickness, pore size of the AAO films, and effective refractive index of liquids. There is a good agreement between the experimental and simulated results, which can help to promote the application of metal-AAO-metal microstructure in reflection filters, images and liquid sensors etc.

1. Introduction

Metal-AAO-metal microstructure has a wide range of promising applications in areas such as surface plasmon resonance [1-2], wavelength absorbers [3-4], RGB display [5-6], optics [7-8], biology [9], chemical sensors [10] and enhanced Raman scattering [11-12]. They exhibit some unique physical and optical properties in the visible spectrum. AAO films display bright structural colors in the visible range when light is incident, and similar phenomena can be observed in nature. For example, both butterflies and insects produce bright structural colors when illuminated by natural light [13-14], which is mainly produced by the interaction between light and matter.

In recent years, ones have finished more experiments [15-17] which were related to optical properties to make a deep understanding of metal-dielectric-metal structure. The Plasmonic microstructure can be used for Coloration of Plastic Consumer Products [18]. Variable interference colors could be achieved by porous alumina-metal layered nano coatings [19]. Many experiments of the color-tuning methods were reported, and the physical mechanism of interference also was analyzed [20-22]. Choi et al. [23] thought optical interference could be effectively coupled with surface plasmon resulting in enhanced optical absorption. However, there are rarely reports about nalyzing the optical reflection from the perspective of simulation and experimental results.

In order to gain a deeper understanding of the interaction between light and matter, AAO films were first prepared using aluminum foil by a two-step anodic oxidation method, followed by vapor deposition of Ag films to obtain Ag-AAO-Al microstructures. A model of the Ag-AAO-Al microstructure was developed using COMSOL to analyze the reflection spectra for different AAO films thicknesses, pore sizes and different kinds of liquids in AAO films. The results show that reflection spectra variations observed in the Ag-AAO-Al microstructure are related to the thickness, pore size and liquids effective refractive index of the AAO films.

2. Experimental

2.1. Sample preparation

Al foils (99.99% purity, 0.20 mm thickness) were first degreased in acetone and ethanol for 5 min and then annealed at 500 °C under vacuum ambient for 2 h to remove the mechanical stress. The first anodization was carried out using a constant voltage of 40 V in 0.3 M oxalic acid at 0 °C for 12 h. The oxide layer formed was then chemically removed by immersing it in the mixed solution of 6.0 wt% H_3PO_4 and 1.8 wt% $H_2Cr_2O_4$ at 60 °C for 24 h. The second anodization was carried out in the same condition. The thickness of AAO films depends on the second anodization time, and the pore size is varied in 5% phosphoric acid. A 15 nm Ag film was then vapor deposited on the samples. The morphology of AAO films was investigated by a field-emission scanning electron microscope (SEM). UV-Vis diffuse reflection spectra of samples viewed at nearly vertical incidence were recorded on a UV-3010 spectrophotometer. Fig. 1 shows the SEM images of the AAO films. Fig. 2 shows the SEM images of the Ag-AAO-Al microstructure.
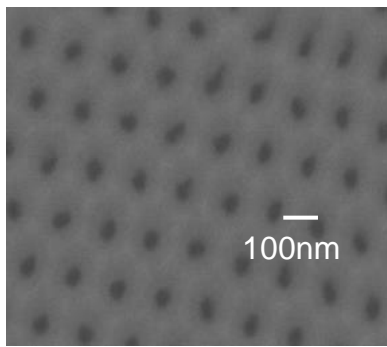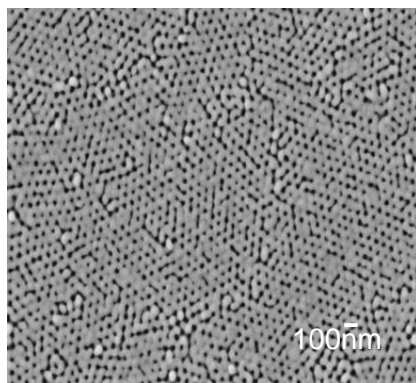
Fig. 1. SEM images of the AAO films

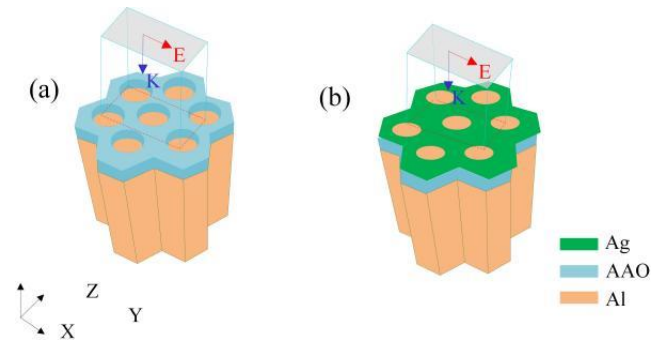Fig. 2. SEM images of the Ag-AAO-Al microstrure

Fig. 3. (a) 3D structure diagram of AAO-Al microstructure (b) 3D structure diagram of Ag-AAO-Al microstructure (color online)
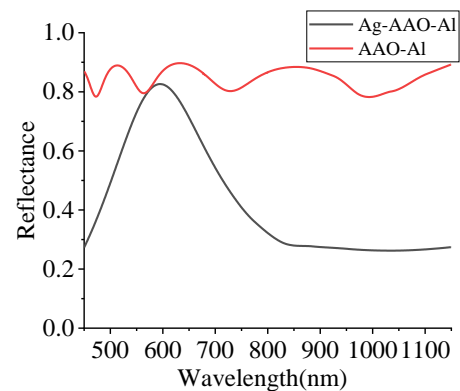

Fig. 4. (a) Simulated reflectance spectrum of Ag-AAO-Al microstructure, (b) Simulated reflectance spectrum of AAO-Al microstructure (color online)

3. Results and discussions

3.1. Influence of Ag nanolayers on its reflection properties

In order to study the influence of the top Ag nanolayers on the optical properties of the Ag-AAO-Al microstructures, the optical roperties of the Ag-AAO-Al microstructures with or without the Ag nanolayer were studied by COMSOL. The AAO layer has a thickness of 100 nm, a pore spacing of 75 nm, a pore size of 30 nm, and a layer of 15 nm Ag is vapor deposited on the top layer of the AAO-Al microstructure. Fig. 3(a) and Fig. 3(b) show the 3D structure diagram of the AAO-Al microstructure and the Ag-AAO-Al microstructure respectively. The plane wave is incident vertically to the surface of the simulated structures. Their reflection spectra are shown in Fig. 4. The electric field distribution enhancement is observed in the Ag-AAO-Al microstructure because the destructive interference pattern (corresponding to the constructive interference in the reflective spectrum) matches with Ag layer, resulting in the weakening of the local surface plasmon resonance compared with that in Ag-AAO-Al microstructure shown in the top panel.

The simulated electric field intensity distribution of the AAO-Al microstructure and Ag-AAO-Al microstructure in the X-Z plane at the center of the nanopore at a specific wavelength is shown in Fig. 5(a) and Fig. 5(b). The electric field distribution enhancement is observed in the Ag-AAO-Al microstructure because of surface plasmon resonance in the thin-film interference.
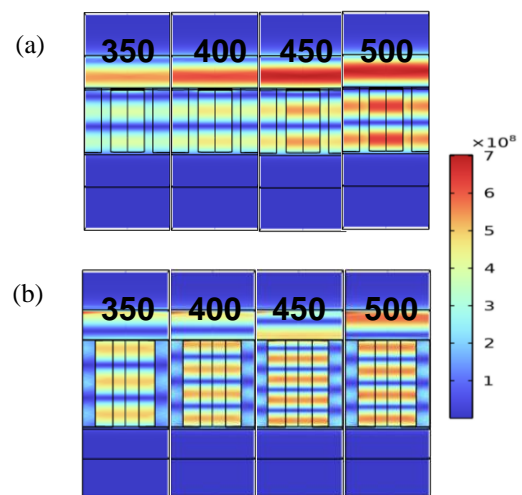

Fig. 5. (a) Electric field distribution (x-z direction) of AAO-Al microstructure at different wavelengths. (b) Electric field distribution (x-z direction) of Ag-AAO-Al microstructure at different wavelengths (color online)

3.2. Effect of different AAO films thicknesses on their reflection properties

The experimental samples with pore size of about 15 nm, pore spacing of about 100 nm, and AAO thickness of about 300 nm and 400 nm were produced by a two-step anodic oxidation method. Then a 15 nm Ag film was vapor deposited on surface of the sanples. The experimental and the simulated reflection spectra of different AAO thicknesses of the Ag-AAO-Al microstructure are shown in Fig. 6(a). Color gamut for structural color display based

on the reflection spectra for Ag-AAO-Al microstructure. The photograph show each color according to the thickness of the AAO films, as shown in Fig. 6(b).

We can observe in Fig. 6(a) that the two results agree well, and the interference peaks are red-shifted as the template thickness changes from 300 nm to 400 nm. For a 300 nm thick AAO film, we also found that the interference peaks occur at 471 nm and 717 nm that the band that corresponds to blue and red, respectively. So they will end up showing a mixture of them as a purple spectrum.
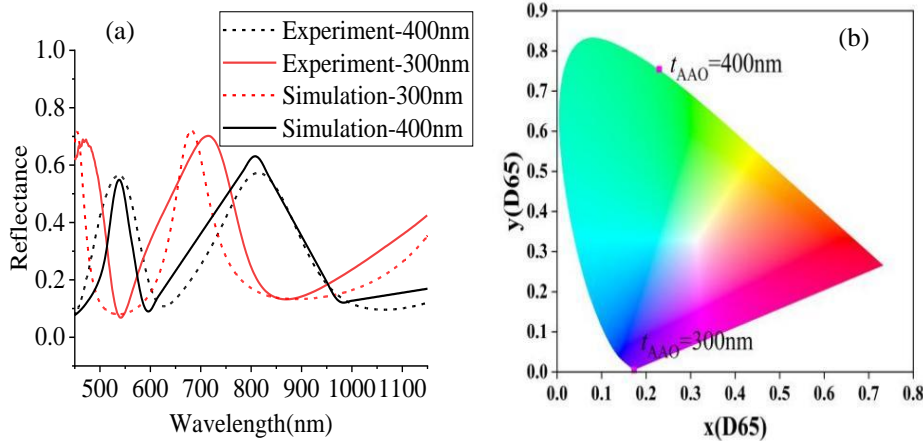

Fig. 6. (a) Experimental and simulated reflection spectra of different AAO thicknesses (b) Representation of Ag-AAO-Al microstructure with different thickness in the CIE 1931color diagram (color online)

3.3. Effect of different pore size of AAO films on their reflection properties

The experimental samples with pore size of about 15 nm and 35 nm, pore spacing of about 100 nm, and AAO thickness of about 300 nm were produced by a two-step anodic oxidation method. Then a 15 nm Ag films was vapor deposited on top. The calculated porosities of these as-prepared AAO films are approximately 0.0816 and

0.4444. The experimental and the simulated reflection spectra of different AAO pore sizes of the Ag-AAO-Al microstructure are shown in Fig. 7(a). Color gamut for structural color display based on the reflection spectra for Ag-AAO-Al microstructure, as shown in Fig. 7(b). We can observe in Fig. 7(a) that the two results agree well, and the interference peaks are red-shifted as the template pore size changes from 15 nm to 35 nm with a shift of up to 89 nm, the reflectance increases from 0.57 to 0.68.
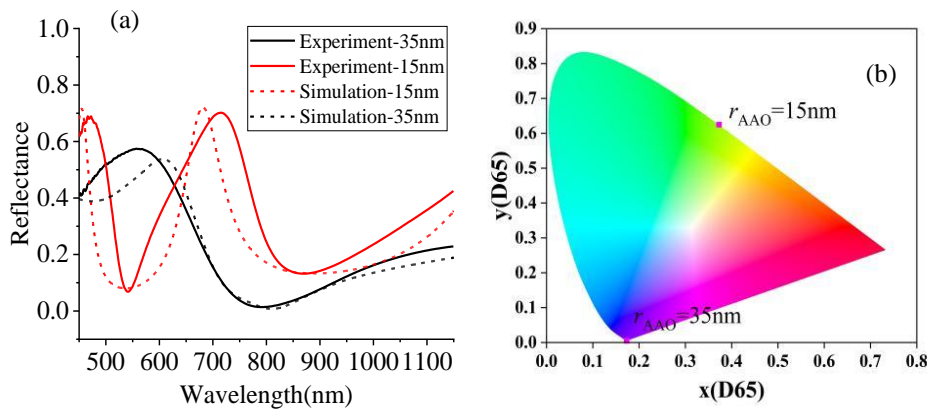

Fig. 7. (a) Experimental and simulated reflection spectra of Ag-AAO-Al microstructures with different pore sizes, (b) Representation of Ag-AAO-Al microstructure with different pore size in the CIE 1931color diagram (color online)

3.4. Effect of different liquids on their reflection properties

Besides changing the structure to tune the color of AAO films, we also use an organic-assisted method to tune the color. In our experiments, the as-prepared AAO films are organophilic for some lower viscosity organics. Therefore, by dripping a series of lower viscosity organics with different refractive indexes into the pores of AAO films with pore size of about 30 nm, pore spacing of about 100 nm, AAO thicknesses of about 400 nm and 15 nm Ag films, we obtained different color of AAO films. The experimental and the simulated reflection spectra of different AAO thicknesses are shown in Fig. 8(a). The color gamut for structural color display is based on the reflection spectra for Ag-AAO-Al microstructure. Fig. 8(b) shows the color gamut diagram of AAO films with an organic infusion. From which we can obviously see that the change of reflection spectra of AAO films. The peak of the interference band shifts from 540 nm to 555 nm after the drop of methanol (n=1.33), the structure color becomes bright green, the peak of the interference band shifts from 540 nm to 579 nm after the drop of acetone (n=1.36), and the structure color changes from blue-green to yellow.
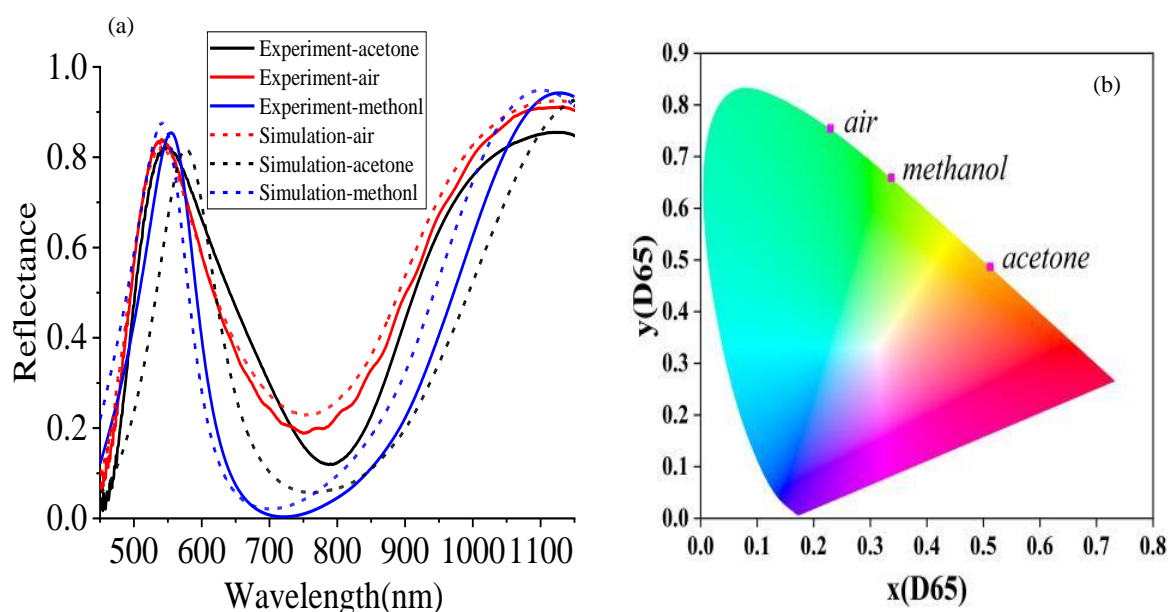

Fig. 8. (a) Experimental and simulated reflection spectra of Ag-AAO-Al microstructure when different organics infused, (b) Representation of Ag-AAO-Al microstructure with different organics infused in the CIE 1931color diagram (color online)

3.5. Discussions

When a beam of light is shining on the AAO films, part of the light will be reflected from the air-Ag interface, the other part will refract into the AAO and be reflected on the AAO-Al interface. The interference between the two beams results in the production of particular colors which correspond to AAO structures. Here the sputtered Ag nanolayer on the AAO surface will enhance the reflectivity of the air-AAO interface. The light reflected from the air-Ag and AAO-Al interfaces will form an effective interference enhancement, and the wavelength (λ) at the maximum reflectance in each interference peak shown in the reflection spectra can be obtained using the Bragg reflector equation [24-25]:

$$\sum 2n_i d_i \cos \theta_i = m\lambda \qquad (1)$$

where n_i is the effective refractive index for every layer i (i = 1, 2, 3, corresponding to the Ag nanolayer, AAO pores, and Al substrate layer separately), d_i is the thickness, and θ_i is the reflection angle of studied layer, m and λ are the order number and reflective peak wavelength, respectively. In our experiments, the morphology and reflection spectra of AAO films investigated are viewed at nearly normal incidence. Hence, the value of θ_i is a constant, and the color (corresponding to wavelength λ) of AAO films is related to the thickness d_i and influential refractive index n_i for every layer.

For a series of AAO films prepared under the same conditions except for anodization time, the pore depths of AAO films (d_2) are the only variable parameter which means that it is straightforward to tune the wavelength of reflection spectra by precisely controlling the pore depth (the anodization time), as described in section 3.2. Moreover, from Fig. 6(a), we can see that the interference

peaks in the visible region red-shift from a short wavelength to a long one with increasing pore depth. The skipping appeared between the pore depth of 300 nm and 400 nm indicates that the new red-shift started which is determined by the order number m, i.e., red-shift occurs in every the same m value and skips when the m changed. So the reflection spectra of the microstructure is sensitive to the pore depth, and this influence will be stronger when the m is small, which is also consistent with Bragg's equation.

According to Eq. (1), the color of AAO films is affected by the influential refractive index n_i of every layer. So the parameters which affect the effective refractive index will affect the reflection spectra of the AAO films. Based on the Maxwell-Garnett theory [26-28], the porous structure can be considered as a homogeneous medium, and the relationship of effective permittivity of AAO layer (ε_{eff}) to the refractive index can be expressed as follows:

$$n_{eff} = \varepsilon_{eff} = F(f, \varepsilon_{air}, \varepsilon_{Al2O3}) \qquad (2)$$

where ε_{air} is the permittivity of air ($n_{air} = 1$), ε_{Al2O3} is the effective permittivity of alumina ($n_{Al2O3} = 1.76$), and f is the porosity of the AAO films. According to Eq. (2), the refractive index of AAO layer (n_2) can be replaced as follows:

$$n = n_{air} \times f + n_{Al2O3} \times (1 - f) \qquad (3)$$

Thus, the effective refractive index n is determined by f. So it is possible to tune color by precisely controlling the f of AAO films which has the following porosity equation [29-30]:

$$f = \frac{2\pi}{\sqrt{3}(r/D_{int})^2} \qquad (4)$$

After the preparation of AAO films, the pore-widen process will enlarge the pore diameters while it cannot affect the interpore distance so that the porosity will change after this process, and the color will change according to the eq. (1) and Eq. (2). The changes of color of AAO films caused by pore diameter on AAO color shown in Fig. 7(b) confirm this point. According to the Eq. (3) it can be concluded that the increase of porosity will decrease the effective refractive index n, so the interference peaks decrease with the porosity increasing. This is called blue-shift in the same m value. At the same time, the effective refractive index of the membrane system is more sensitive to porosity and pore depth than the Ag layer. Therefore the fine-tuning color can be realized by only adjusting the widened process time, and the interference peaks of AAO films in the visible region show a blue-shift with increasing porosity, which follows the Bragg's equation.

As for the different colors of AAO films by diverse organics infusion, the shift of interference peaks can be ascribed to the increase of effective refractive index n according to Eq. (3). As described in Fig. 8, the changes of interference peaks are different for different structural AAO films with organics infusion according. In addition, the color of AAO films with large pore depth and porosity is obviously changed when absorbed organics with different refractive index.

4. Conclusion

In summary, the experimental samples were prepared by the two-step anodic oxidation method and vapor deposition. The reflection spectra of different AAO film thicknesses, pore sizes, and organics infused were studied. The results show that the experimental and simulation results were in good agreement, which fully verified the experimental results from the simulation point of view. The interference peaks of AAO films in the visible region shift from a shorter wavelength to a long one by increasing the pore depth, decreasing the porosity, and increasing the refractive index of organics absorbed into their porous. We believe that this work can not only lead to a better understanding of the optical interference mechanism of this microstructure and improve the interaction between light and matter. This vivid microstructure may apply reflection filters, RGB displays, liquid sensors, etc.

References

[1] D. Choi, C. K. Shin, D. Yoon, D. S. Chung, Y. W. Jin, L. P. Lee, Nano Letters **6**(14), 3374 (2014).
[2] T. J. Palinski, A. Tadimety, I. Trase, B. E. Vyhnalek, G. W. Hunter, E. Garmire, J. X. Zhang, Optics Express **16**(29), 25000 (2021).
[3] D. Oller, G. E. Fernandes, S. Siontas, J. Xu, D. Pacifici, Materials Research Bulletin **83**(100), 556 (2016).
[4] Y. Huang, F. Lv, J. Chen, S. He, Z. Wang, J. La, D. Wu, R. Cong, Y. Wang, W. Wang, Nanotechnology **13**(33), 135302 (2022).
[5] D. Franklin, R. Frank, S.-T. Wu, D. Chanda, Nature Communications **1**(8), 15209 (2017).
[6] J. Carneiro, F. Machado, M. Pereira, V. Teixeira, M. Costa, A. Ribeiro, A. Cavaco-Paulo, A. Samantilleke, RSC Advances **65**(8), 37254 (2018).
[7] L. Wang, X. Qin, D. Ji, J. P. Parry, J. Zhang, C. Deng, G. Ding, Q. Gan, H. Zeng, X. Xu, Applied Surface Science **355**(100), 139 (2015).
[8] N. Loan, N. Anh, Optoelectron. Adv. Mat. **2**(15), 71 (2021).

[9] P.-H. Lo, G.-L. Luo, W. Fang, 2015 28th IEEE International Conference on Micro Electro Mechanical Systems (MEMS) **3**, 69 (2015).

[10] J. Lee, J. Kim, M. Lee, Nanoscale Advances **10**(2), 4930 (2020).

[11] J. Hu, L. Chen, Z. Lian, M. Cao, H. Li, W. Sun, N. Tong, H. Zeng, The Journal of Physical Chemistry C **29**(116), 15584 (2012).

[12] C.-S. Park, S.-S. Lee, ACS Applied Nano Materials **4**(4), 4216 (2021).

[13] M. Shaban, Journal of Nanomaterials **1**(16), 417 (2015).

[14] C. Ma, W. Ren, L. Wang, Optoelectron. Adv. Mat. **2**(13), 104 (2019).

[15] M. Pashchanka, S. Yadav, T. Cottre, J. J. Schneider, Nanoscale **21**(6), 12877 (2014).

[16] C. Manzano, J. Best, J. Schwiedrzik, A. Cantarero, J. Michler, L. Philippe, Journal of Materials Chemistry C **32**(4), 7658 (2016).

[17] L. Wang, X. Qin, D. Ji, J. P. Parry, J. Zhang, C. Deng, G. Ding, Q. Gan, H. Zeng, X. Xu, Applied Surface Science (355), 139 (2015).

[18] J. S. E. Clausen, A. B. Christiansen, S. Yazdi, M. Grajower, H. Taha, U. Levy, A. Kristensen, N. A. Mortensen, Nano Letters **8**(14), 4499 (2014).

[19] L. Liang, T. Zhang, K. Wang, H. Tang, X. Yang, X. Zhu, Y. Duan, H. Li, Applied Optics **4**(53), 544 (2014).

[20] M. Seo, J. Kim, H. Oh, M. Kim, I. U. Baek, K. D. Choi, J. Y. Byun, M. Lee, Advanced Optical Materials **13**(7), 1900196 (2019).

[21] J. Lee, J. Kim, M. Lee, Nanoscale Advances **10**(2), 4930 (2020).

[22] H. Wang, L. Huang, Y. Zhang, Y. Cai, L. Cheng, L. Zhai, Y. Liu, X. Zhang, J. Zhu, Optical Materials Express **6**(12), 2270 (2022).

[23] D. Choi, C. K. Shin, D. Yoon, D. S. Chung, Y. W. Jin, L. P. Lee, Nano Letters **6**(14), 3374 (2014).

[24] X. Wang, D. Zhang, H. Zhang, Y. Ma, J. Jiang, Nanotechnology **30**(22), 305306 (2011).

[25] Q. Xu, Y. Yang, J. Gu, Z. Li, H. Sun, Materials Letters **74**(74), 137 (2012).

[26] J. M. Garnett, Philosophical Transaction of the Royal Society of London. Series A, Containing Papers of a Mathematical of Physical Character **359-371**(203), 385 (1904).

[27] J. Hohlbein, U. Rehn, R. Wehrspohn, Physica Status Solidi (a) **4**(201), 803 (2004).

[28] G. Hornyak, C. Patrissi, E. Oberhauser, C. Martin, J. Valmalette, L. Lemaire, J. Dutta, H. Hofmann, Nanostructured Materials **1-8**(9), 571 (1997).

[29] A. Reina, H. Son, L. Jiao, B. Fan, M. S. Dresselhaus, Z. Liu, J. Kong, The Journal of Physical Chemistry C **46**(112), 17741 (2008).

[30] W. Yan-qing, W. Gao-feng, H. Qing-gong, F. Liang, G. Shi-rong, Procedia Earth and Planetary Science **1**(1), 1513 (2009).

_____

*Corresponding author: T20070600@csuft.edu.cn